ELSEVIER

Chemical Physics 253 (2000) 27–40

Chemical Physics

www.elsevier.nl/locate/chemphys

The electronic structure of rare-earth oxides in the creation of the core hole

Chikashi Suzuki [a,*], Jun Kawai [b], Masao Takahashi [c], Aurel-Mihai Vlaicu [a], Hirohiko Adachi [b], Takeshi Mukoyama [a]

[a] *Institute for Chemical Research, Kyoto University Uji, Kyoto 611-0011, Japan*

[b] *Department of Materials Science and Engineering, Kyoto University, Sakyo-ku, Kyoto 606-8501, Japan*

[c] *The Institute of Scientific and Industrial Research, Osaka University, Mihogaoka 8-1, Ibaragi, Osaka 567-0047, Japan*

Received 30 July 1999

Abstract

We studied the electronic structures of rare-earth sesqui-oxides R_2O_3 (R: rare-earth element) with a core hole, both experimentally and theoretically. The experimental study was made by measuring the rare-earth 3d X-ray photoemission spectra (XPS) of these oxides. Clear double-peak structures were observed for La_2O_3, the shoulder or broad foot of the low-binding-energy side of 3d XPS were observed for Pr_2O_3, Nd_2O_3, and Sm_2O_3, and single-peak structures were observed for Eu_2O_3, Gd_2O_3, and Dy_2O_3. The calculation of electronic structures was performed for the ground state and the $3d^{-1}$ core-hole states by the spin-unrestricted DV-Xα molecular-orbital method for model clusters chosen as $[RO_6]^{9-}$ for R_2O_3. The calculated results show the difference of the electronic structure in the ground state and the core-hole states. In the creation of the core hole, the number of unpaired 4f electrons increases by less than one due to the weak charge-transfer effect for La_2O_3 and Ce_2O_3, and this corresponds to the clear double-peak structure of the rare-earth 3d XPS. For Eu_2O_3 and Yb_2O_3, the number increases and decreases by less than 1 due to the restricted charge-transfer effect by filling $4f^{\uparrow}$ and 4f orbitals with electrons. Due to the strong charge-transfer effect, the number of unpaired 4f electrons increase by more than 1 for Pr–Sm oxides, and this effect produces, the shoulder or broad foot in the low-binding-energy side of the rare-earth 3d XPS peak. The decrease by more than 1 for Gd–Tm oxides results in clear single peak structures. The present results indicate that rare-earth sesqui-oxides can be classified into the four groups by spin response.

1. Introduction

Rare-earth compounds show interesting physical properties such as mixed valency, a heavy fermion, and Kondo-like behaviors due to the interaction between the localized 4f electrons and delocalized conduction bands. Electron spectroscopies, such as X-ray photoemission spectroscopy [1–9], bremsstrahlung isochromat spectroscopy [2–4], X-ray absorption spectroscopy [2,3], and electron-energy-loss spectroscopy [8] are effective to study 4f electronic states of rare-earth compounds and have clarified the physical origin of their interesting properties, described above. Especially, the core-hole X-ray photoemission

* Corresponding author. Present address: Metallic Material Department, Material Technology Laboratory, Fujikura Ltd., 1-5-1, Kiba, Koto-ku, Tokyo 135-0042, Japan.

E-mail address: csuzuki@rd.fujikura.co.jp (C. Suzuki).

0301-0104/00/$ - see front matter
PII: S0301-0104(99)00380-8

spectrum (XPS) is a powerful tool to investigate the electronic states of rare-earth compounds. In experimental core-hole XPS, the existence of a core hole plays an important role. When a core hole is created, the localized 4f level is pulled down by the attractive Coulomb potential of the suddenly created core hole and, the relaxation of the 4f charge distribution occurs through the hybridization between the 4f states and the valence (conduction) states in order to screen the core hole. Tanaka and Kotani [10] called this phenomenon valence-mixing relaxation. The valence-mixing relaxation effects cause characteristic spectral structures in the XPS. These structures are attributed to the first-order optical process [10].

It was especially interesting that the double-peak structures have been observed in both the rare-earth $3d_{5/2}$ and $3d_{3/2}$ core-level spectra of some rare-earth compounds [1,11–19]. The intensity ratio of the high- to low-binding-energy peaks showed a dramatic change for rare-earth sesqui-oxides (R_2O_3), for R = La, Ce, Pr, and Nd [11,17–19]. Each of the double peaks corresponds to the bonding or the antibonding state in the final state. However, the quantitative information for such changes has not been obtained directly from the experimental spectra. It was reported that, for Sm_2O_3, the double-peak structure disappears and changes to the single peak [20–22]. The rare-earth 3d XPS of Eu_2O_3–Tm_2O_3 were also studied [22]. However, the rare-earth 3d XPS of Sm–Tm oxides reported in various papers were measured with different instruments in different experimental conditions. In addition, for Eu_2O_3–Tm_2O_3, quite a few experimental data of rare-earth 3d XPS have been reported. Therefore, in order to compare the spectra of rare-earth oxides, it is necessary to measure the spectra with the same instrument in similar conditions.

Theoretically, the core-hole XPS of these rare-earth oxides have been interpreted [23–26] within the Gunnarsson–Schonhammer model [3–5] of the Anderson impurity Hamiltonian [27]. However, in this model, some parameters and measured values were needed to obtain wave functions of the initial and final states. The wave functions of the core-hole state have, especially been found only with some fitting parameters, and these parameters are decided arbitrarily to fit the theoretical spectra to the experimental spectra.

To understand core-hole XPS, it is necessary to know the difference of the electronic state between the ground state and the core-hole state among the compounds. In particular, for rare-earth compounds, it is important to take into consideration the charge transfer from ligand to rare-earth 4f orbitals in the creation of the core hole. To estimate the difference of the electronic states in the ground and the core-hole state among rare-earth sesqui-oxides without experimental results and fitting parameters, it is necessary to perform the first-principle calculation.

We have already clarified the difference of the electronic states in the ground state and the core-hole state among La halides and oxides [28], and showed that the intensity ratios of La 3d XPS of these compounds correspond to the charge-transfer effect, according to ligand changes. In the case of La halides [1,12], there are two results for the spectra measured with the same instrument in the same condition. The fact allows one to establish these spectra and to compare them with the theoretical results. However, it is not the case for some rare-earth oxides. In addition, it is necessary to show quantitative information directly from the experimental spectra in order to check or compare with the results of the first-principles calculation.

In this work, we study the electronic structures of the rare-earth oxides in the presence of a core hole. For this purpose, we measure the rare-earth 3d XPS of rare-earth oxides and perform the first-principles calculation. From the obtained results, the difference of the electronic state in the ground and the core-hole state among the rare-earth sesqui-oxides is clarified and the relations of such difference and the rare-earth 3d XPS of these oxides is obtained. We apply the method developed by Kawai and coworkers for 3d transition-metal oxides [29,30] by the spin response in the creation of the core hole, to the case of rare-earth oxides and classify them with the spin response of 4f orbital in the creation of the 3d core hole and show the correlation between the classification and the experimental results.

2. Experiment

We measured rare-earth 3d XPS of La_2O_3, Pr_2O_3, Nd_2O_3, Sm_2O_3, Eu_2O_3, Gd_2O_3, and Dy_2O_3. The powder samples of rare-earth sesqui-oxides with 99.9% purity for Pr_2O_3, and 99.99% for Nd_2O_3, Sm_2O_3, Eu_2O_3, Gd_2O_3, and Dy_2O_3 were commercially obtained from Soekawa Chemistry Co. Ltd., and those with 99.99% for La_2O_3 were obtained from Furuuchi Chemistry Co., Ltd. A sample of Pr_2O_3 was prepared by smearing powder directly on to a conductive tape adhesive. Samples of other oxides were prepared as pellets annealed at 1000°C for 12 h. All samples were measured immediately after the sample preparation to avoid deterioration of samples. XPS measurements were conducted at the Material Analysis Center, the Institute of Scientific and Industrial Research, Osaka University. The instrument we used was Microlabo Mark III made by VG Scientific, Ltd. The photon sources used were Mg Kα ($h\nu = 1253.6$ eV) and Al Kα ($h\nu = 1486.6$ eV). All binding energies were referenced to the main C 1s component (aliphatic hydrocarbon) at 285.0 eV.

3. Experimental results

The typical examples of the observed rare-earth 3d XPS spectra of rare-earth sesqui-oxides are shown in Fig. 1. For La_2O_3 (Fig. 1(a)), there are clearly a pair of two separate peaks in La 3d XPS. The shape of La $3d_{5/2}$ and La $3d_{3/2}$ spectra resemble each other. The 3d spectra for Pr and Nd oxides have a similar shape, but only the latter is

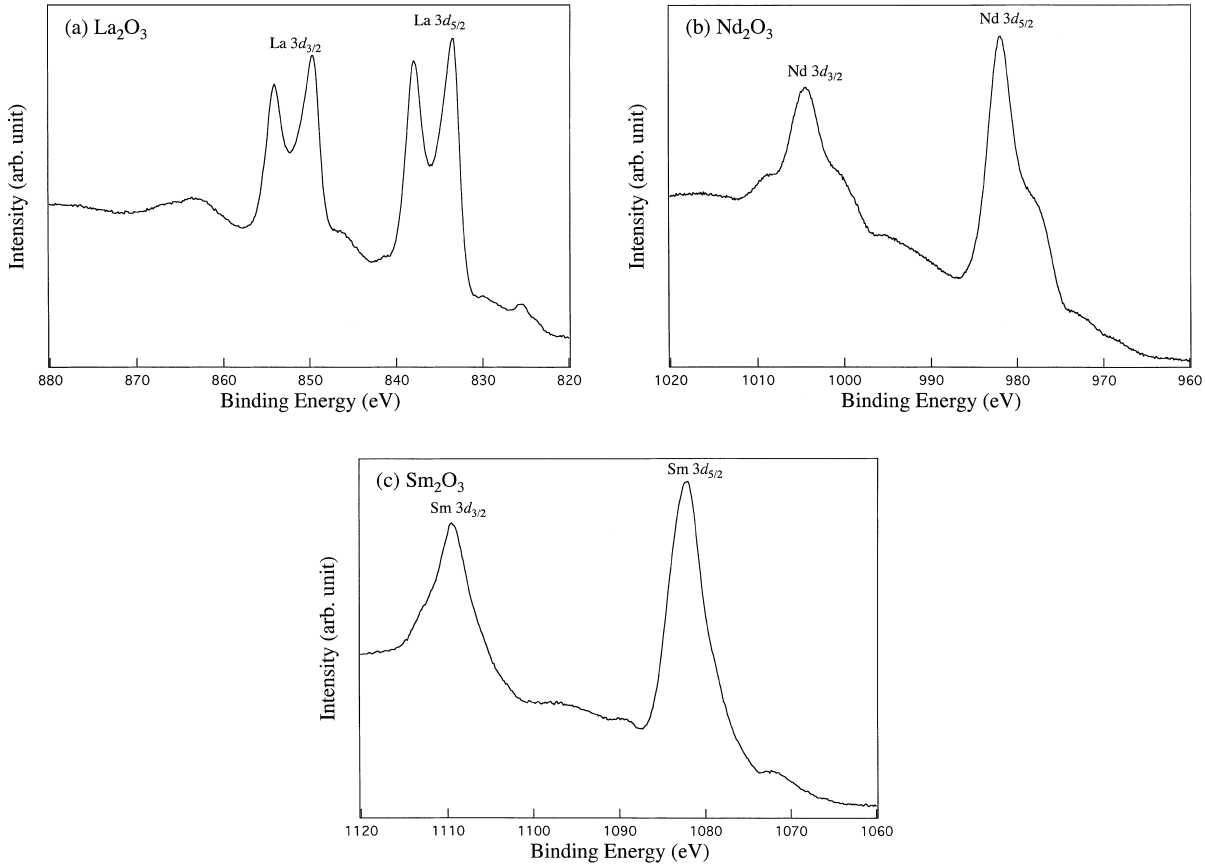

Fig. 1. Observed rare-earth 3d X-ray photoemission spectra for (a) La_2O_3, (b) Nd_2O_3, and (c) Sm_2O_3.

plotted in Fig. 1(b). There is a shoulder on the low-energy-side of the peak of both Pr and Nd 3d XPS. Further, the other shoulders are observed at the high-energy side of $3d_{3/2}$, as reported previously for Pr_2O_3 [20]. Except for such shoulders as found in the $3d_{3/2}$ region, the difference between the shapes of $3d_{5/2}$ and $3d_{3/2}$ for both oxides is not remarkable. As the peak shape is not so different in Sm_2O_3, Eu_2O_3, Gd_2O_3, and Dy_2O_3, we show only the 3d XPS for Sm_2O_3 in Fig. 1(c). The shape of the rare-earth $3d_{3/2}$ spectra for these oxides is mostly similar to that of the corresponding $3d_{5/2}$ spectra.

For all oxides, satellites are observed at about 10 eV lower binding energy side from the $3d_{5/2}$ peak. They are caused by the $K\alpha_{3,4}$ line of the photon source. Other satellites are observed at about 10 eV higher binding energy side from the $3d_{5/2}$ peak. These satellites are thought to be the energy-loss peaks. The energy-loss peaks of rare-earth trihalides are discussed in detail in Ref. [1]. However, such peaks are not remarkable for Pr_2O_3 and Nd_2O_3. This is because the energy-loss peaks of $3d_{5/2}$ and the satellite of $3d_{3/2}$ attributed to the $K\alpha_{3,4}$ line of photon source are located close to each other.

For simplicity, we discuss only the rare-earth $3d_{5/2}$ region. Two components have been extracted by a Lorenzian-function fitting of the $3d_{5/2}$ region. The intensity ratios of the high- to low-binding-energy peak were estimated to be 1.02, 2.06, and 2.38 for La_2O_3, Pr_2O_3, and Nd_2O_3. The value for Ce_2O_3 was estimated to be 1.4 from the reported spectra [18] by comparing the peak heights. For Sm_2O_3, the double-peak structure disappears and changes to the single peak, but the foot on the low-binding-energy side of $3d_{5/2}$ line is broad. For Eu_2O_3, Gd_2O_3, and Dy_2O_3, no distinct satellite is observed in our measurements except for the satellites due to both $K\alpha_{3,4}$ line of photon source and the energy loss, and a clear single peak is observed.

4. Calculations

To clarify the effect of the creation of the core hole, we have calculated the electronic structures of both the ground state and the $3d^{-1}$ core-hole states for model clusters, using the DV-Xα molecular-orbital method [31]. The model clusters contained one rare-earth atom and neighboring oxygen atoms and were taken as $[RO_6]^{9-}$ (R = La–Nd, Sm–Gd, and Dy–Yb). The basis sets used were, the rare-earth 1s–6p, and O 1s–2p. These model clusters have an O_h symmetry, and the geometry of these model clusters is given in Table 1. The bond length of each cluster is the average of lengths between the central atom and the first sixth- or seventh-nearest atom as in Sm–Yb–O [32], or La–O [33], Ce–O, Pr–O, and Nd–O [32].

Table 1
Oxides and their corresponding clusters

Oxide	Model cluster	Cluster symmetry	Bond length (Å)	Reference
La_2O_3	$[LaO_6]^{9-}$	O_h	2.54	[33]
Ce_2O_3	$[CeO_6]^{9-}$	O_h	2.59	[32]
Pr_2O_3	$[PrO_6]^{9-}$	O_h	2.26	[32]
Nd_2O_3	$[NdO_6]^{9-}$	O_h	2.27	[32]
Sm_2O_3	$[SmO_6]^{9-}$	O_h	2.24	[32]
Eu_2O_3	$[EuO_6]^{9-}$	O_h	2.23	[32]
Gd_2O_3	$[GdO_6]^{9-}$	O_h	2.22	[32]
Dy_2O_3	$[DyO_6]^{9-}$	O_h	2.19	[32]
Ho_2O_3	$[HoO_6]^{9-}$	O_h	2.22	[32]
Er_2O_3	$[ErO_6]^{9-}$	O_h	2.17	[32]
Tm_2O_3	$[TmO_6]^{9-}$	O_h	2.14	[32]
Yb_2O_3	$[YbO_6]^{9-}$	O_h	2.14	[32]

Kimura et al. [34] calculated silicon clusters of various sizes, and summarized the effect of cluster size. Kaneyoshi et al. [35] compared X-ray emission spectra of graphite calculated by the large cluster model with those by the small one. In these calculations, the effect of cluster size did not give fundamentally different results, even though the wave functions of their valence band are delocalized. Therefore, we adopted the model clusters containing one rare-earth atom and neighboring oxygen atoms as shown above.

The number of random sampling points in the DV-Xα calculations was 2100, 300 points per atom. Slater's exchange parameter (α) was fixed at 0.7 for all the atoms in the cluster. All atoms were situated in a well potential of radius 4.0 bohrs (1 bohr = 0.529 Å) and depth −2.0 hartrees (1 hartree = 27.2 eV) to converge the atomic basis sets for negatively charged clusters.

5. Calculated results and discussion

5.1. Densities of states

To clarify the behavior of 4f orbitals of rare-earth oxides in the creation of the core hole with the unempirical method, we used the DV-Xα molecular-orbital method [31].

We first show the calculated electron densities of states of the rare-earth 4f and 5d–6p, and O 2p components in the ground state, in the $3d\downarrow^{-1}$ core-hole state, and in the $3d\uparrow^{-1}$ core-hole state for Ce oxide in Fig. 2, and those in the ground state and in the $3d\downarrow^{-1}$ core-hole state for Nd, Eu, and Tm oxides in Figs. 3–5 in order to see the electronic structures. The plotted density of states (DOS) have been reduced to R–O (equivalent atomic percent) instead of RO_6 (R: rare earth atom); O DOSs were reduced to one-sixth to compare the DOS between rare earth and O on the same scale. The gross atomic-orbital populations [36] of the rare-earth 4f, and 5d–6p, and O 2p are plotted against the molecular orbital Xα energy in Figs. 2–5, where the level width is broadened by a Lorenzian function (0.5 eV full width at half maximum) to mimic the solid state.

We have omitted the DOSs of the $3d\uparrow^{-1}$ core-hole state except for Ce oxide, though we calculated them. The reasons are the following: For Tm and Yb oxides, their spins are simply reversed to the spins of the $3d\downarrow^{-1}$ core-hole state. For Nd and Sm oxides, the energy of the unoccupied 4f↓ components in the $3d\uparrow^{-1}$ core-hole state is lower than that in the $3d\downarrow^{-1}$ core-hole state by 0.7 eV, but the other differences between the electronic structures in both core-hole states are negligible. For Eu and Gd oxides, the shapes of the DOSs of the $3d\uparrow^{-1}$ and $3d\downarrow^{-1}$ core-hole state are almost the same.

In the case of Ce oxide, the difference between the energies of the unoccupied Ce 4f components in the $3d\uparrow^{-1}$ and $3d\downarrow^{-1}$ core-hole states cannot be ignored, and therefore, for example, the difference between the spin states in both the core-hole states is significant, as shown later. Therefore, we show both the DOSs in the $3d\uparrow^{-1}$ and $3d\downarrow^{-1}$ core-hole states only for Ce oxide.

We had already discussed La oxides in our previous article [28]. The electronic structures of Pr oxides are similar to those of Nd oxides. Moreover, for Gd–Tm oxide, there are some differences among the electronic structures of these oxides, but they are not remarkable. We do not show the DOSs of La, Pr, Dy, Ho, and Er oxides.

The spin configuration of $[TmO_6]^{9-}$ is reversed from the ground state in the $3d\uparrow^{-1}$ core-hole state, which is not true for other model clusters, but is conserved in the $3d\downarrow^{-1}$ core-hole state. Therefore, it is more useful to compare DOSs in the ground state with DOSs in the $3d\downarrow^{-1}$ core-hole state than in the $3d\uparrow^{-1}$ core-hole state. For this reason, we discuss only the $3d\downarrow^{-1}$ core-hole state as the core-hole state except $[CeO_6]^{9-}$ though we have calculated $3d\uparrow^{-1}$ core-hole state. Moreover, this is the reason why we use the $3d\downarrow^{-1}$ core-hole state as the core-hole state to calculate the intensity ratios of two components in the rare-earth $3d_{5/2}$ region, as shown later.

For $[CeO_6]^{9-}$, $[NdO_6]^{9-}$, and $[SmO_6]^{9-}$, most of the rare-earth 4f↓ components are almost empty. For these clusters, little charge is transferred to the rare-earth 4f↓ components in the creation of the core hole except for $[CeO_6]^{9-}$, but such charge transfer is not remarkable for $[CeO_6]^{9-}$. On the contrary, the rare-earth 4f↑ components are hybridized with O 2p components especially in the core-hole state and some charge is transferred to the rare-earth 4f↑ components in the creation of the core hole. Therefore, we consider only the rare-earth 4f↑ and O 2p components for $[CeO_6]^{9-}$, $[NdO_6]^{9-}$, and $[SmO_6]^{9-}$. For $[GdO_6]^{9-}$ and $[TmO_6]^{9-}$, the rare-earth 4f↑ components are hybridized with O 2p but filled with electrons, and no charge was transferred to 4f↑ components in the creation of the core hole. Therefore, we consider only the rare-earth 4f↓ and O 2p components for $[GdO_6]^{9-}$ and $[TmO_6]^{9-}$.

As shown in Fig. 2, Ce 4f components are hybridized with O 2p components in the core-hole state though those in the ground state are little hybridized. The energy of unoccupied 4f↓ components of $[CeO_6]^{9-}$ in the $3d\uparrow^{-1}$ core-hole state is lower than in the $3d\downarrow^{-1}$ core-hole state by 0.7 eV, which is of the same value as those of $[NdO_6]^{9-}$ and $[SmO_6]^{9-}$. However, less 4f electrons are occupied for $[CeO_6]^{9-}$ than for other clusters, and the difference between the energies of the rare-earth

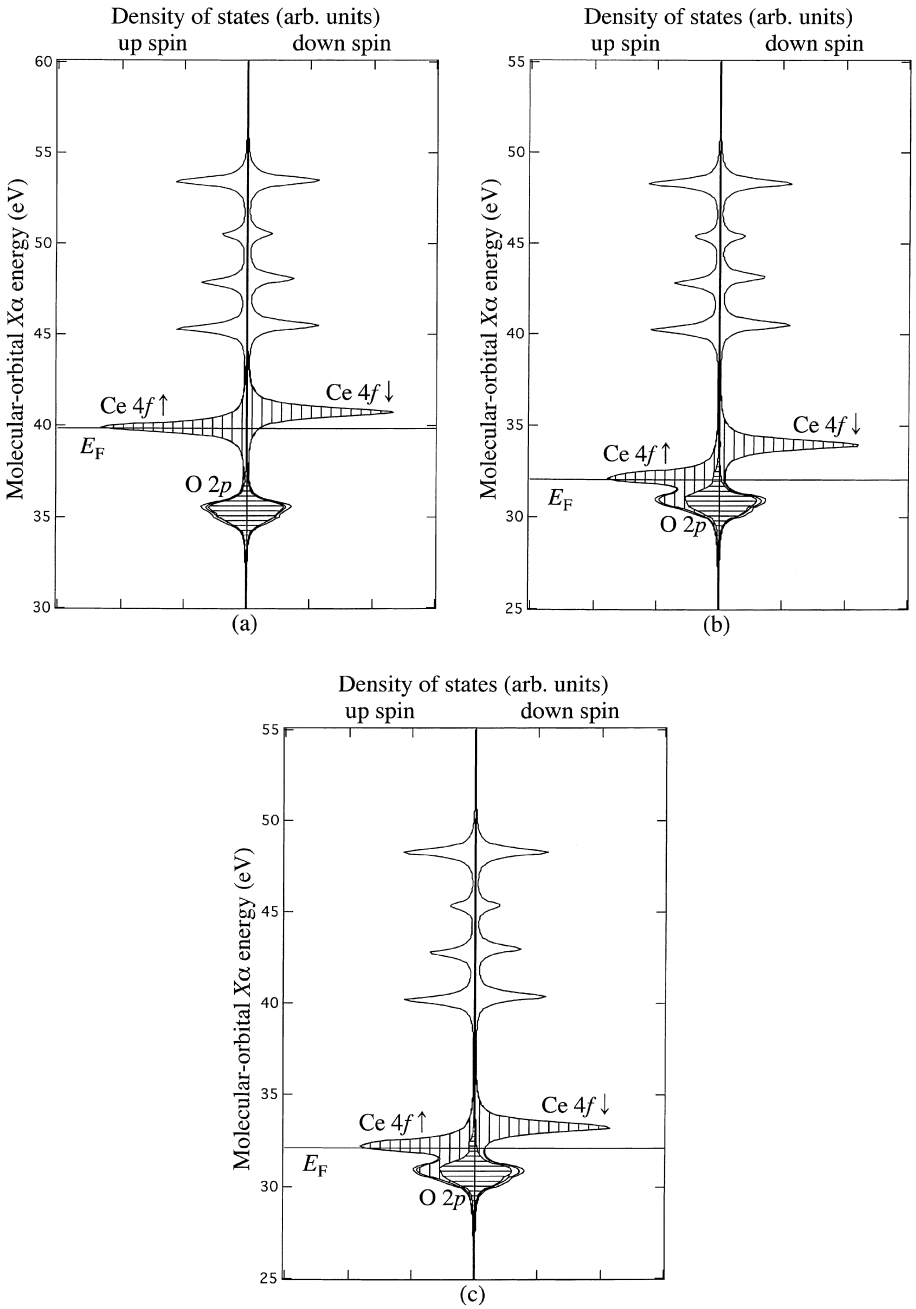

Fig. 2. Calculated Ce 4f, 5d, 6s, and 6p and O 2p DOS of $[CeO_6]^{9-}$ cluster in the (a) ground state, (b) the $3d\downarrow^{-1}$ core-hole state, and (c) $3d\uparrow^{-1}$ core-hole state. Horizontally hatched range: O 2p, vertically hatched range: Ce 4f, full range: Ce 4f, 5d, 6s, and 6p, and O 2p.

4f↑ and 4f↓ components of $[CeO_6]^{9-}$ is smaller than those of these clusters. Therefore, the difference between the charge-transfer effects in the creation of the $3d\uparrow^{-1}$ and $3d\downarrow^{-1}$ core holes is much larger for $[CeO_6]^{9-}$.

The Nd 4f↑ components are hybridized with the O 2p components in the core-hole state, though those in the ground state are a little hybridized as well as the Ce 4f↑ components. However, the energy of the O 2p components is similar to that of the Nd 4f↑ components and this hybridization of $[NdO_6]^{9-}$ is stronger than that of $[CeO_6]^{9-}$ in the core-hole state.

As shown in Fig. 3, in the ground state, Sm 4f↑ components are somewhat hybridized with O 2p, which is not true for Ce and Nd oxides. In the core-hole state, Sm 4f↑ components are hybridized with O 2p components strongly, and the energy of Sm 4f↑ components is a little lower than that of O 2p components, and Sm 4f↑ components are nearly filled with electrons due to charge transfer. Therefore, O 2p components of Sm oxide are larger than that of Ce and Nd oxides above Fermi level in the core-hole state. In addition to this result, for Sm_2O_3, the foot of the low-binding-energy side of $3d_{5/2}$ line is broadened, as described before. From this calculated result, it is thought that the low-binding-energy peak is very small and hidden in the foot of the high-binding-energy peak.

From the results for Ce, Pr, Nd, and Sm, it can be said that the more the rare-earth atomic number increases, the deeper the rare-earth 4f components become in the creation of the core hole, compared with O 2p components.

The results for Eu are shown in Fig. 4. The Eu 4f↑ components are hybridized strongly with O 2p in the ground state. In the core-hole state, the energy of Eu 4f↑ components of $[EuO_6]^{9-}$ becomes much deeper than $[CeO_6]^{9-}$, $[NdO_6]^{9-}$, and $[SmO_6]^{9-}$, compared with O 2p components. As a result, Eu 4f↑ components are filled with electrons and the ligand hole is created in O 2p components. Moreover, some charge is transferred to the Eu 4f↓ components. From this fact, the energy of the Eu 4f↑ components are crossed with the energy of the O 2p components completely in the creation of the core hole.

In the case of Gd oxide, the Gd 4f↓ components are strongly hybridized with O 2p in the core-hole state, though those in the ground state are little hybridized. In addition, the energy of Gd 4f↓ components is a little higher than that of O 2p components, but, as a whole, DOSs of the Gd 4f↓

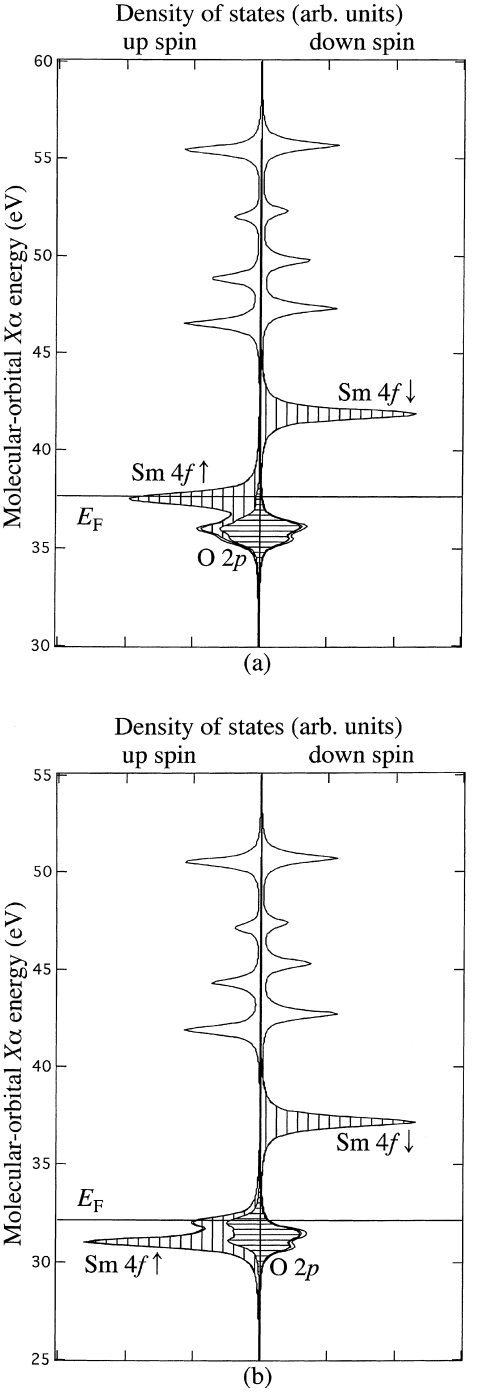

Fig. 3. Calculated Sm 4f, 5d, 6s, and 6p and O 2p DOS of $[SmO_6]^{9-}$ cluster in (a) the ground state and (b) the $3d\downarrow^{-1}$ core-hole state. Horizontally hatched range: O 2p, vertically hatched range: Sm 4f, full range: Sm 4f, 5d, 6s, and 6p, and O 2p.

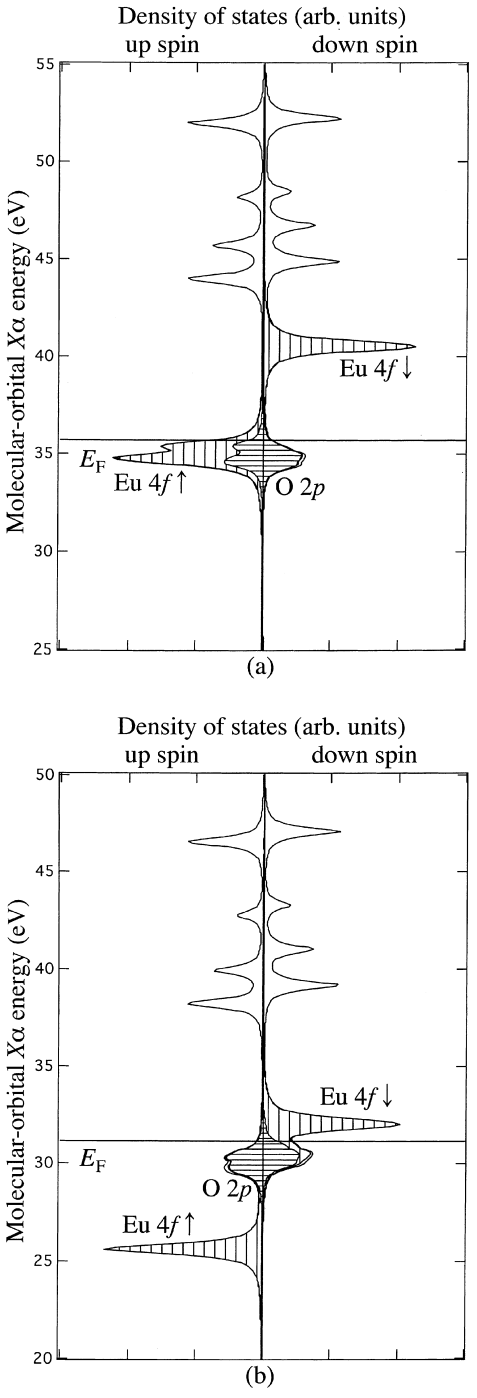

Fig. 4. Calculated Eu 4f, 5d, 6s, and 6p and O 2p DOS of $[EuO_6]^{9-}$ cluster in (a) the ground state and, (b) the $3d\downarrow^{-1}$ core-hole state. Horizontally hatched range: O 2p, vertically hatched range: Eu 4f, full range: Eu 4f, 5d, 6s, and 6p, and O 2p.

and O 2p↓ components can be regarded as similar to DOSs of Nd 4f↑ and O 2p↑ components in the core-hole state. However, the Gd $3d_{5/2}$ line is a single peak. This is because the hybridization strength between rare-earth 4f and O 2p [26] becomes weak due to lanthanide contraction.

As shown in Fig. 5, in the ground state, Tm 4f↓ components are somewhat hybridized, which is not true for Gd oxides. In the core-hole state, Tm 4f↓ components are hybridized with O 2p components strongly. In addition, the energy of Tm 4f↑ components is a little lower than that of O 2p components, and Tm 4f↑ components are nearly filled with electrons due to charge transfer. Therefore, O 2p components of Tm oxide are larger than those of Gd oxides above Fermi level in the core-hole state.

For $[DyO_6]^{9-}$, $[HoO_6]^{9-}$, and $[ErO_6]^{9-}$, the characteristics of electronic structure are intermediate between $[GdO_6]^{9-}$ and $[TmO_6]^{9-}$, and we think there are no important characteristics to discuss in detail.

For $[YbO_6]^{9-}$, the Yb 4f↑ and 4f↓ components are hybridized strongly with O 2p components in the ground state. In the core-hole state, the energy of the Yb 4f↓ components becomes much deeper than $[GdO_6]^{9-}$ and $[TmO_6]^{9-}$, compared with O 2p components. As a result, Yb 4f components are filled with electrons and the ligand hole is created in O 2p components. From this fact, the energy of Yb 4f components is completely crossed with the energy of O 2p components in the creation of the core hole, similar to the case of Eu_2O_3.

5.2. The energy deepening of the rare-earth 4f and O 2p components

The calculated values of the energy deepening of the rare-earth 4f and O 2p components in the creation of the $3d\downarrow^{-1}$ core hole are shown in Table 2. The energy of O 2p components becomes deeper in the creation of the $3d\downarrow^{-1}$ core hole by 4.1–5.0 eV for all oxides except for Ho oxide, which is by 3.8–3.9 eV. (These values are similar except for Ho oxide.) The energy deepening of O 2p components for Ho oxide is a little smaller than those for other oxides.

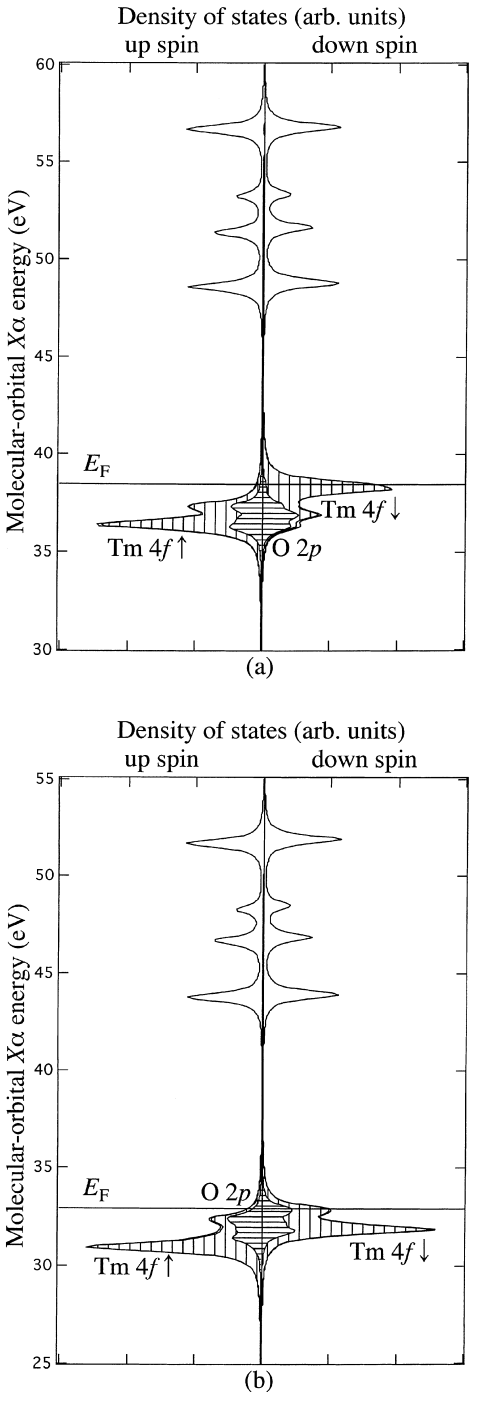

Fig. 5. Calculated Tm 4f, 5d, 6s, and 6p and O 2p DOS of $[TmO_6]^{9-}$ cluster in (a) the ground state and (b) the $3d\downarrow^{-1}$ core-hole state. Horizontally hatched range: O 2p, vertically hatched range: Tm 4f, full range: Tm 4f, 5d, 6s, and 6p, and O 2p.

The energy deepening of O 2p components is smaller than the rare-earth 4f components for all oxides in the creation of the $3d\downarrow^{-1}$ core hole. This indicates that the core-hole Coulomb attraction is more influential on the rare-earth 4f components than on O 2p components.

The energy deepening of the rare-earth 4f↑ components is larger than the 4f↓ components for Ce–Eu oxides, but this tendency is reversed for Gd–Yb oxides. This is because the 4f↓ components for Ce–Eu oxides or 4f↑ components for Gd–Yb oxides are almost empty or completely filled with electrons and little or no charge is transferred to these components in the creation of the core hole and 4f↓–4f↓ or 4f↑–4f↑ exchange interaction dose not increase for Ce–Eu or Gd–Yb oxides. From these results, we discuss only the 4f↑ components for La–Eu oxides and the 4f↓ components for Gd–Yb oxides.

The value of the energy deepening of 4f↑ or 4f↓ is 6–8 eV for La–Sm or Gd–Tm oxides, and this ordering of 4f↑ components is $[LaO_6]^{9-} > [CeO_6]^{9-} > [PrO_6]^{9-} > [NdO_6]^{9-} = [SmO_6]^{9-}$ and that of 4f↓ components is $[GdO_6]^{9-} = [HoO_6]^{9-} > [DyO_6]^{9-} = [ErO_6]^{9-} = [TmO_6]^{9-}$. From this fact, the ordering of the screening of core-hole Coulomb attraction by O 2p electrons is $[LaO_6]^{9-} < [CeO_6]^{9-} < [PrO_6]^{9-} < [NdO_6]^{9-} = [SmO_6]^{9-}$ or $[GdO_6]^{9-} = [HoO_6]^{9-} < [DyO_6]^{9-} = [ErO_6]^{9-} = [TmO_6]^{9-}$. This indicates the ordering of the hybridization of the rare-earth 4f and O 2p; in other words, the electron correlation order is $La_2O_3 < Ce_2O_3 < Pr_2O_3 < Nd_2O_3 = Sm_2O_3$ or $Gd_2O_3 = Ho_2O_3 < Dy_2O_3 = Er_2O_3 = Tm_2O_3$. This ordering corresponds to the rare-earth atomic number, but the case of Ho_2O_3 is exceptional.

The energy deepening of Ho 4f↓ or O 2p components of Ho_2O_3 is larger or smaller than what is expected from the rare-earth atomic number. For H_2O_3, Ho 4f↓ and O 2p components play more or less important roles to screen the core hole than what is thought as a function of rare-earth atomic number. For Eu or Yb oxide, the energy deepening of the rare-earth 4f components is 9–10 eV and remarkably larger than for other oxides. This is because the Eu 4f↑ components of Eu oxide or the Yb 4f components of Yb oxide are filled with electrons in the creation of the core hole, and less

Table 2
Value of the energy deepening of the rare-earth 4f and O 2p components in the creation of the $3d\downarrow^{-1}$ core hole (in eV)

Oxide	Model cluster	Rare-earth 4f↑	O 2p↑	Rare-earth 4f↓	O 2p↓
La_2O_3	$[LaO_6]^{9-}$	8.1	4.3	7.4	4.4
Ce_2O_3	$[CeO_6]^{9-}$	7.9	4.3	6.7	4.5
Pr_2O_3	$[PrO_6]^{9-}$	7.0	4.2	5.7	4.5
Nd_2O_3	$[NdO_6]^{9-}$	5.9	4.2	4.4	4.5
Sm_2O_3	$[SmO_6]^{9-}$	6.2	4.3	4.7	4.6
Eu_2O_3	$[EuO_6]^{9-}$	9.4	4.7	8.5	4.3
Gd_2O_3	$[GdO_6]^{9-}$	7.5	4.7	7.8	4.5
Dy_2O_3	$[DyO_6]^{9-}$	6.1	4.8	6.6	4.5
Ho_2O_3	$[HoO_6]^{9-}$	7.1	3.8	7.5	3.9
Er_2O_3	$[ErO_6]^{9-}$	5.6	4.7	6.2	4.5
Tm_2O_3	$[TmO_6]^{9-}$	5.6	4.8	6.1	4.5
Yb_2O_3	$[YbO_6]^{9-}$	9.8	5.0	10.2	4.8

charge is transferred to the rare-earth 4f components of Eu or Yb oxide than those of other oxides from O 2p components. Therefore, the rare-earth 4f and O 2p components in these calculations play more or less important roles to screen the core hole than do other clusters.

Core-hole Coulomb attraction energies to the rare-earth 4f state from the Anderson impurity model of rare-earth oxides were estimated to be 11–13 eV [26], which indicate that the core-hole effects were similar among these oxides. On the contrary, the energy deepening of unoccupied 4f components in our calculations is much smaller than these values. This is because the model clusters were simple and the calculation was nonrelativistic. Also, the similarity among core-hole Coulomb attraction energies of various rare-earth oxides which have an effect on the rare-earth 4f states in the Anderson impurity model was thought to be attributed to the negligence of the core-hole creation effect to the O 2p components.

5.3. The correspondence of the peak intensity ratios to the charge-transfer effect and the classification of rare-earth oxides

The double-peak structures of the 3d XPS are observed for La, Ce, Pr, and Nd oxides, as described above. This structure can be ascribed to the charge-transfer effect from the ligand to the rare-earth 4f orbitals due to the creation of the 3d vacancy. The peak corresponding to a lower binding energy corresponds to the bonding orbital in the final state, whereas, that for a higher binding energy, to the antibonding orbital.

In rare-earth compounds, the ground state is expressed as

$$|\mathrm{g}\rangle = a_0|4\mathrm{f}^n\rangle + b_0|4\mathrm{f}^{n+1}\underline{L}\rangle + \cdots,$$

where n represents nominal number of 4f electrons and $\underline{L}$ the ligand hole in O 2p. On the contrary, the final state are the bonding or antibonding state of $|4\mathrm{f}^n\underline{c}\rangle, |4\mathrm{f}^{n+1}\underline{L}\ \underline{c}\rangle$, and so on configuration ($\underline{c}$ represents a core hole), and expressed as, respectively

$$|\mathrm{f}_1\rangle = a|4\mathrm{f}^n\underline{c}\rangle + b|4\mathrm{f}^{n+1}\underline{L}\ \underline{c}\rangle + \cdots,$$

$$|\mathrm{f}_2\rangle = b|4\mathrm{f}^n\underline{c}\rangle - a|4\mathrm{f}^{n+1}\underline{L}\ \underline{c}\rangle + \cdots$$

In the sudden approximation, the photoemission spectrum is represented [10] by

$$F(E_B) = \sum_i |\langle \mathrm{f}_i|\mathrm{g}\rangle|^2 \frac{\Gamma/\pi}{(E_B - \Delta E_i)^2 + \Gamma^2},$$

where $|\mathrm{f}_i\rangle$ represents the core-hole state (final state), Γ represents half width at half max (HWHM), and ΔE_i represents the difference between the energy of the ground state (initial state) $|\mathrm{g}\rangle$ and that of the core-hole state (final state) $|\mathrm{f}_i\rangle$. Therefore, the intensity ratios of the high- to low-binding-energy peak represents

$$\frac{I_{\mathrm{high}}}{I_{\mathrm{low}}} = \frac{|\langle \mathrm{f}_2|\mathrm{g}\rangle|^2}{|\langle \mathrm{f}_1|\mathrm{g}\rangle|^2}.$$

The details of the calculated intensity ratio were shown in the review of Ref. [37] and in our previous paper [28].

In Table 3, we show the calculated intensity ratios of the high- to low-binding-energy peak, which are 0.49, 0.56, 0.67, and 0.73 for La_2O_3, Ce_2O_3, Pr_2O_3, and Nd_2O_3, considering only 7–9t_{1u}, and 1, 2t_{2u} level because the effects of other levels are minor. We use the $3d\downarrow^{-1}$ core-hole state as the core-hole state to calculate the intensity ratios. This was already discussed earlier. The observed ordering of the intensity ratios is $Nd_2O_3 > Pr_2O_3 > Ce_{2O_{3d}} > La_2O_3$ and has the same tendency as the calculated one, though the calculated ratios are much smaller than the measured ratios because of the simplicity of models and the negligence of relativistic effects.

As pointed out by Kawai and coworkers [29,30,38], the difference between the numbers of unpaired 3d electrons in the ground state and the core-hole state was a good index of the charge-transfer effect in 3d transition-metal compounds; in a similar way, we consider the quantity of $|4f\uparrow–4f\downarrow|$ in the ground state and the $3d^{-1}$ core-hole state.

In order to clarify the correspondence of the intensity ratio of the double-peak structures to the charge-transfer effects, we list the relation between the measured and calculated intensity ratios, and the numbers of unpaired 4f electrons in the ground state and the $3d\downarrow^{-1}$ core-hole state in Table 3. The numbers of unpaired 4f electrons in the $3d\downarrow^{-1}$ core-hole state increase from the ground state by 0.48, 0.86, 1.08, and 1.24 for La, Ce, Pr, and Nd oxides. From this fact, it is found that the charge-transfer effect order is $La_2O_3 < Ce_2O_3 < Pr_2O_3 < Nd_2O_3$ in the creation of the core hole. We can find that the intensity ratios correspond to the charge-transfer effect.

Table 3
Calculated effective number of unpaired 4f electrons and intensity ratio of the rare-earth $3d_{5/2}$ XPS

Oxide Model cluster	La_2O_3 $[LaO_6]^{9-}$	Ce_2O_3 $[CeO_6]^{9-}$	Pr_2O_3 $[PrO_6]^{9-}$	Nd_2O_3 $[NdO_6]^{9-}$
Ground state	0.00	1.03	2.07	3.18
$3d\downarrow^{-1}$ core-hole state	0.48	1.89	3.15	4.42
Observed ratio	1.02	1.4	2.06	2.38
Calculated ratio	0.49	0.56	0.67	0.73

To see the charge-transfer effect of all oxides, we list the numbers of $|4f\uparrow–4f\downarrow|$ in the ground state and the $3d^{-1}$ core-hole state in Table 4. The calculated effective numbers of 4f unpaired electrons ($4f\uparrow–4f\downarrow$) in the ground state are almost nominal values for La, Ce, Pr, Gd, and Ho oxides, and intermediate values between those of $|4f^n\rangle$ and $|4f^{n+1}\rangle$ for Sm, Eu, Er, Tm, and Yb oxides. The spin states of the $3d\uparrow^{-1}$ and $3d\downarrow^{-1}$ core-hole state for La, Tm, and Yb oxides are reversed to each other. Therefore, the numbers of unpaired 4f electrons in both core-hole states are equal for these oxides. For Ce oxide, the difference between the numbers of unpaired 4f electrons in the $3d\uparrow^{-1}$ and in the $3d\downarrow^{-1}$ core-hole state is remarkably larger than the other oxides, as described before. However, the numbers of unpaired 4f electrons in both core-hole states are those of intermediate $|4f^n\rangle$ and $|4f^{n+1}\rangle$. The difference between the numbers of unpaired 4f electrons in the $3d\uparrow^{-1}$ and $3d\downarrow^{-1}$ core-hole states for Pr oxides is 0.1 and those for Nd–Er sesqui-oxides is less than 0.1. These values showed that whether the spin of the 3d core hole is up or down is almost out of the question for these oxides from the point of the charge-transfer effect. The electronic states in the $3d^{-1}$ core-hole state for Pr, Eu, Gd, Dy, Ho, and Yb oxides are almost $|4f^{n+1}\rangle$, and those for Sm, Nd, Er, and Tm oxides are intermediate between $|4f^{n+1}\rangle$ and $|4f^{n+2}\rangle$.

In Fig. 6, we have plotted the correlation between the calculated number of unpaired 4f electrons of rare-earth in the ground and the $3d^{-1}$ core-hole state. The solid straight line in this figure indicates the conservation of spin state. The broken line indicates the increase or decrease of the number of unpaired 4f electrons by one in the creation of the $3d^{-1}$ core hole. The difference between the numbers of unpaired 4f electrons in the ground state and in the $3d^{-1}$ core-hole state is less than one for La_2O_3, Ce_2O_3, Eu_2O_3, and Yb_2O_3. Moreover, for La_2O_3 and Ce_2O_3, the ground state is expressed as $|4f^n\rangle$ and the $3d^{-1}$ core-hole state is expressed as

$$a_1|3d^{-1}\ 4f^n\rangle + b_1|3d^{-1}\ 4f^{n+1}\ \underline{L}\rangle,$$

Table 4
Calculated effective number of unpaired 4f electrons

Oxide	Model cluster	Nominal number	Ground state	$3d\uparrow^{-1}$ hole state	$3d\downarrow^{-1}$ hole state
La_2O_3	$[LaO_6]^{9-}$	0	0.00	0.48	0.48
Ce_2O_3	$[CeO_6]^{9-}$	1	1.03	1.63	1.89
Pr_2O_3	$[PrO_6]^{9-}$	2	2.07	3.04	3.15
Nd_2O_3	$[NdO_6]^{9-}$	3	3.18	4.37	4.42
Sm_2O_3	$[SmO_6]^{9-}$	5	5.21	6.37	6.41
Eu_2O_3	$[EuO_6]^{9-}$	6	6.44	6.62	6.67
Gd_2O_3	$[GdO_6]^{9-}$	7	6.89	5.82	5.88
Dy_2O_3	$[DyO_6]^{9-}$	5	4.84	3.68	3.73
Ho_2O_3	$[HoO_6]^{9-}$	4	3.96	2.88	2.93
Er_2O_3	$[ErO_6]^{9-}$	3	2.76	1.58	1.63
Tm_2O_3	$[TmO_6]^{9-}$	2	1.73	0.59	0.59
Yb_2O_3	$[YbO_6]^{9-}$	1	0.78	0.00	0.00

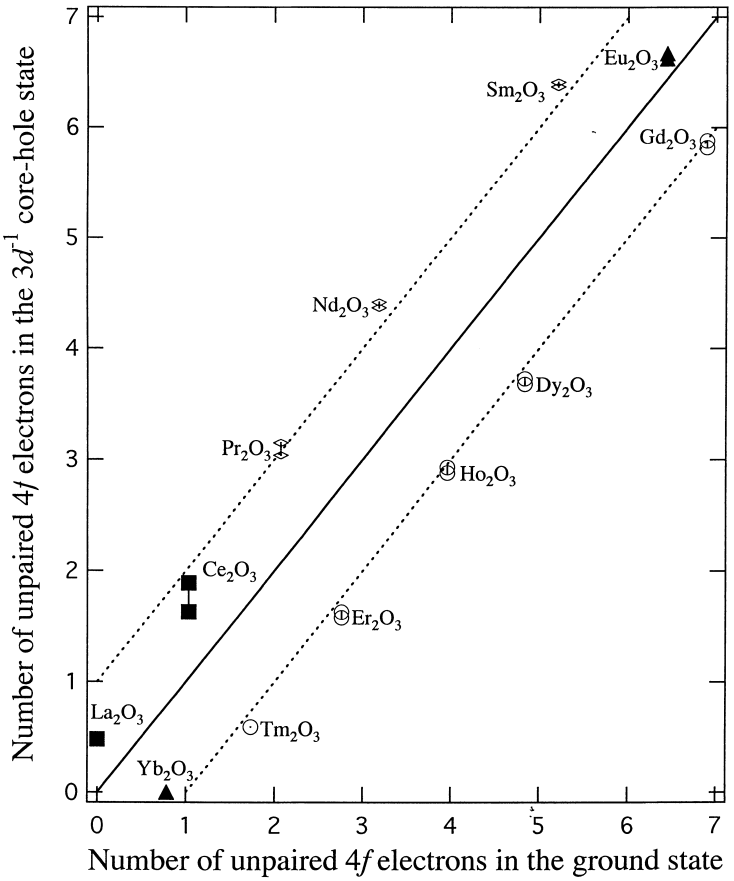

Fig. 6. Plot of the calculated number of unpaired 4f electrons in the ground state and the $3d^{-1}$ core-hole states. The $3d^{-1}$ core-hole is either the $3d\uparrow^{-1}$ or the $3d\downarrow^{-1}$ core-hole for each oxide.

where $\underline{L}$ denotes the ligand hole in O 2p. The charge transfer occurred weakly for these oxides, which are indicated by solid squares. These compounds show the clear double-peak structure of the rare-earth 3d XPS. For Eu_2O_3 and Yb_2O_3, the ground state is expressed as

$$a_0|4f^n\rangle + b_0|4f^{n+1}\ \underline{L}\rangle,$$

and the $3d^{-1}$ core-hole state is expressed as

$$|3d^{-1}\ 4f^{n+1}\underline{L}\rangle.$$

The charge transfer is restricted by filling 4f↑ or 4f components with electrons in the creation of the core hole for these oxides, which are indicated by solid triangles. For Pr_2O_3, Nd_2O_3, Sm_2O_3, the numbers of unpaired 4f electrons increase by more than one in the creation of the $3d^{-1}$ core hole. The ground state is expressed as

$$a_0|4f^n\rangle + b_0|4f^{n+1}\ \underline{L}\rangle,$$

and the $3d^{-1}$ core-hole state is expressed as

$$b_1|3d^{-1}\ 4f^{n+1}\ \underline{L}\rangle + c_1|3d^{-1}\ 4f^{n+2}\ \underline{L}^2\rangle.$$

For Pr_2O_3, since $|b_0|^2$ and $|c_1|^2$ is small, the ground state and the $3d^{-1}$ core-hole state are expressed as almost $|4f^n\rangle$ and $|3d^{-1}\ 4f^{n+1}\ \underline{L}\rangle$, respectively. The charge transfer occurred strongly in these oxides in the creation of the core hole. These oxides are indicated by an open rhombus and show the shoulder or broad foot of the low-binding-energy side of the rare-earth 3d XPS. For Gd–Tm sesqui-oxides, the numbers of unpaired 4f electrons decrease in a creation of the $3d^{-1}$ core-hole state by more than one. The ground state and the core-hole state are expressed in a similar way to Pr–Sm sesqui-oxides. Moreover, for Gd_2O_3 and Ho_2O_3, the ground state and the $3d^{-1}$ core-hole state are expressed in a manner similar to that for Pr_2O_3. The charge transfer occurred strongly in these oxides in the creation of the core hole. These oxides are indicated by open circles. However, they show the clear single peak structures of the rare-earth 3d XPS because of weak hybridization strength between rare-earth 4f and O 2p due to lanthanide contraction. Consequently, it is now clear that the response in the creation of the core hole is a measure of classification of the rare-earth oxides into the four groups. This classification reflects the change of the rare-earth 3d XPS among rare-earth oxides.

6. Conclusions

We measured the rare-earth 3d XPS of rare-earth oxides and calculated their electronic structures. From the measurement, it is found that the shapes of the rare earth $3d_{5/2}$ spectra show a dramatic change for La–Sm oxides and that no distinct satellite is observed for Eu–Dy oxides.

The calculations of the electronic structures were performed with respect to the ground state and the $3d^{-1}$ core-hole state, using spin unrestricted DV-Xα method with cluster model approximation. The calculated results clarified the difference of the electronic structure in the ground state and the core-hole states among various rare-earth sesqui-oxides. With respect to La–Nd oxides, where the double-peak structures are observed in rare-earth 3d region, the calculated intensity ratio of two peaks has the same ordering as the experimental one. Therefore the ordering of XPS intensity ratios was explained by these calculations. In addition, from the increase in the numbers of unpaired 4f electrons in the creation of the core hole, it is shown that the shapes of the rare-earth 3d XPS correspond to the charge-transfer effect.

We also calculated for other oxides and could classify rare-earth oxides into the four groups: In the first group, oxides containing La_2O_3 and Ce_2O_3 showed that the numbers of unpaired 4f electrons increase in the creation of the $3d^{-1}$ core hole by less than one due to the weak charge-transfer effect. The second group consists of Eu_2O_3 and Yb_2O_3 and the numbers of unpaired 4f electrons increase and decrease in the creation of the $3d^{-1}$ core hole by less than one due to the restricted charge-transfer effect by filling 4f↑ and 4f orbitals with electrons. The third one containing Pr_2O_3, Nd_2O_3, and Sm_2O_3 showed that the numbers of unpaired 4f electrons increase in the creation of the $3d^{-1}$ core hole by more than one, due to the strong charge-transfer effect. The fourth contains Gd–Tm sesqui-oxides and the numbers of unpaired 4f electrons decrease in the creation of

the $3d^{-1}$ core hole by more than one, due to the strong charge-transfer effect like the third one. This classification reflects the change of the shape of the rare-earth 3d XPS. It was found in the present study that the core-hole calculation is a method useful to classify the rare-earth oxides.

Acknowledgements

We would like to thank Dr. Y. Ito for his continuous encouragement during the work.

References

[1] K.H. Park, S.-J. Oh, Phys. Rev. B 48 (1993) 14833.
[2] J.W. Allen, S.-J. Oh, O. Gunnarsson, K. Schonhammer, M.B. Maple, M.S. Torikachvili, I. Lindau, Adv. Phys. 35 (1986) 275.
[3] O. Gunnarsson, K. Schonhammer, Phys. Rev. Lett. 50 (1983) 604.
[4] O. Gunnarsson, K. Schonhammer, Phys. Rev. B 28 (1983) 4315.
[5] O. Gunnarsson, K. Schonhammer, Phys. Rev. B 31 (1985) 4815.
[6] S.-H. Liu, K.M. Ho, Phys. Rev. B 26 (1982) 7052.
[7] S.-H. Liu, K.M. Ho, Phys. Rev. B 28 (1983) 4220.
[8] E. Wuilloud, B. Delly, W.D. Schneider, Y. Baer, Phys. Rev. Lett. 53 (1984) 202.
[9] N.E. Bickers, D.L. Cox, J.W. Wilkins, Phys. Rev. Lett. 54 (1985) 230.
[10] S. Tanaka, A. Kotani, J. Phys. Soc. Jpn. 61 (1992) 4212.
[11] A.J. Signorelli, R.G. Heyes, Phys. Rev. B 8 (1973) 81.
[12] S. Suzuki, T. Ishii, T. Sagawa, J. Phys. Soc. Jpn. 37 (1973) 1334.
[13] A. Fujimori, Phys. Rev. B 27 (1983) 3992.
[14] S. Imada, T. Jo, Phys. Scr. 41 (1990) 115.
[15] S. Imada, T. Jo, J. Phys. Soc. Jpn. 58 (1989) 402.
[16] S. Imada, T. Jo, J. Phys. Soc. Jpn. 58 (1989) 2665.
[17] J.C. Fuggle, M. Campagna, Z. Zolnierek, R. Lässer, A. Platau, Phys. Rev. Lett. 45 (1980) 1597.
[18] J.W. Allen, J. Magn. & Magn. Mater. 47 & 48 (1985) 168.
[19] H. Ogasawara, A. Kotani, R. Potze, G.A. Sawatrzky, B.T. Thole, Phys. Rev. B 44 (1991) 5465.
[20] M. Aono, S. Kawai, S. Kono, M. Okusawa, T. Sagawa, Y. Takehara, Solid State Commun. 16 (1974) 13.
[21] R.S. Mulliken, Chem. Phys. Lett. 15 (1976) 433.
[22] T. Takahashi, M. Fujinami, H. Arai, S. Hashiguchi, T. Ohtsubo, Autum meeting of Phys. Soc. Japan, 6a C3-17, 1988.
[23] W.D. Schneider, B. Delley, E. Wuilloud, J.M. Imer, Y. Baer, Phys. Rev. B 32 (1985) 6819.
[24] A. Kotani, M. Okada, T. Jo, A. Bianconi, A. Marcell, J.C. Parleba, J. Phys. Soc. Jpn. 56 (1987) 798.
[25] T. Nakano, A. Kotani, J.C. Parleba, J. Phys. Soc. Jpn. 56 (1987) 2201.
[26] T. Ikeda, K. Okada, H. Ogasawara, A. Kotani, J. Phys. Soc. Jpn. 59 (1990) 622.
[27] P.W. Anderson, Phys. Rev. 124 (1961) 41.
[28] C. Suzuki, T. Mukoyama, J. Kawai, H. Adachi, Phys. Rev. B 57 (1998) 9507.
[29] J. Kawai, C. Suzuki, H. Adachi, J. Electron Spectrosc. Relat. Phenom. 78 (1996) 79.
[30] C. Suzuki, J. Kawai, H. Adachi, T. Mukoyama, submitted for publication.
[31] H. Adachi, S. Shiokawa, M. Tsukuda, C. Satoko, S. Sugano, J. Phys. Soc. Jpn. 47 (1979) 1528.
[32] R.W.G. Wykoff, Crystal Structures II, 2nd ed., Tucson, Aizona, 1986, pp. II-1–6.
[33] A.F. Well, Structural Inorganic Chemistry, 5th ed., Oxford University Press, Oxford, 1984, pp. 543–547.
[34] H. Kimura, S. Imanaga, Y. Hayafuji, H. Adachi, Adv. Quant. Chem. 29 (1997) 193.
[35] T. Kaneyoshi, Y. Kowada, T. Tanaka, J. Kawai, M. Motoyama, Spectrochim. Acta B 54 (1999) 189.
[36] R.S. Mulliken, J. Chem. Phys. 23 (1955) 1833.
[37] A. Kotani, H. Ogasawara, J. Electron Spectrosc. Relat. Phenom. 60 (1992) 257.
[38] J. Kawai, C. Suzuki, H. Adachi, T. Konishi, Y. Gohshi, Phys. Rev. B 50 (1994) 11347.